Technology and Health Care 13 (2006) 1–18 1
IOS Press

Finite element stress analysis of cuneiform and cylindrical threaded implant geometries

Mauro Cruz[a,*,1], Adelino Francisco Lourenço[b], Elson Magalhães Toledo[c,d], Luis Paulo da Silva Barra[d], Afonso Celso de Castro Lemonge[d] and Thomaz Wassall[e]

[a]*Clinest – Clinical Center of Research in Stomatology, São Leopoldo Mandic Research Center, Dental School, Av. Rio Branco, 2288 – 1205 – Juiz de Fora, MG, 36016-310, Brazil*
Tel./Fax: +55 32 3215 3957; E-mail: clinest@terra.com.br
[b]*Private Practice, São Paulo, SP, Brazil*
[c]*Computational Mechanics Coordination, LNCC, Petrópolis, RJ, Brazil*
[d]*UFJF – Federal University of Juiz de Fora, School of Engineering Campus, Cidade Universitária, Juiz de Fora, MG, Brazil*
[e]*São Leopoldo Mandic Research Center, Dental School, R. José Rocha Junqueira 13, Ponte Preta, Campinas, SP, Brazil*

Abstract. *Statement of problem.* Different implant geometries present different biomechanical behaviors and in this context, one arising question is how cuneiform implant geometry compares to clinical successful cylindrical threaded implant geometry.

Purpose. The purpose of this work was to study stress distribution around cuneiform and cylindrical threaded implant geometries using three-dimensional finite element stress analysis taking the latter as a reference.

Material and methods. A model was generated from a computerized tomography of a human edentulous mandible with implants placed in the left first premolar region. The model was supported by the mastication muscles and by temporomandibular joint. A vertical load of 100N was applied at the top of each implant in the direction of their long axes. The mandibular boundary conditions were modeled considering the actual muscle supporting system. Taking muscle forces intensities and directions, balance moment equations were employed to assess the system equilibrium. Cortical and medullary bones were assumed to be homogeneous, isotropic and linearly elastic.

Results. The analysis provided results for maximum (S1) and minimum (S2) principal stress and Von Mises (SEQV) stress field. For both geometries, the results showed concentration on one side of the neck, smooth stress distribution along the body and no considerable concentration at the apical area.

Conclusion. Results showed similar stress distribution pattern for cuneiform and cylindrical threaded geometries. The stresses profiles along the implants length reproduced their morphology. In both occurred stress concentration at one side of the neck and no body or apical stress concentration.

Keywords: Biomechanics, dental implants, dental stress analysis, finite element analysis

[1]The first author is a scientific consultant for the Maxtron Co., which funded the grant for this research.
*Corresponding author.

1. Introduction and literature review

Since the introduction of osseointegration concept [3,10], cylindrical threaded implant geometry described by Brånemark et al. [10–12], has been a reference for many studies. This implant is well known and documented in clinic and laboratory situations in several long-term studies, which provided reliability and assurance to its use, in this way becoming the gold standard of the implant technique [5, 26,29,46,52,54,55].

In the last years, some studies have focused on the implants biomechanical behavior [1,4,6–8,18–20,23, 41,43,45,46,51–55,62,65,66] and most of these works included this geometry, comparing it to different geometries. Biomechanical behavior is not only strictly dependent on implant geometry, but also on its design, including shape, dimension and material, as well as the prostheses [13,14,59]. However, since nowadays all implant system employs quite similar material and prostheses features for all prosthetic implant solutions, the study of the surrounding bone stress distribution and its dependency on implant shapes, brings valuable contribution to the improvement of implant's geometry and biomechanical behavior [58]. The use of finite element method (FEM) in this mechanical analysis of dental implants has been described by many authors [1,6,8,9,18–20,43–46,52,54,55,59,61,62,66]. This method presents suitable degree of reliability and accuracy "without the risk and expense of implantation" as pointed out by Cook et al. [19]. However, the degree of accuracy of the FEM results depends on how the model agrees with actual anatomic structures and physiologic conditions [27,31,33,34,36,37]. Previous attempts in modeling the implant-bone relationship often use two-dimensional analysis [51,53,55,66]. It has been demonstrated in some different studies that the three-dimensional (3-D) approach, the modeling of the boundary conditions around the implant considering different degrees of bone-implant contact [9, 20], the presence of cortical or medullary bone [40,46] and the use of more refined models, can produce more reliable results [27,33,34,41,42,52,54]. Quantitative comparison between analyses under different modeling conditions are not reliable due to the sensitivity of the model parameters in the results [27]. Similar conditions have to be provided in order to obtain reliable results [28].

Different from the natural tooth, the implant interface is a rigid contact that transmits occlusal loads directly to the adjacent bone that can produces high levels of stress concentration [5]. Previous studies showed that this concentration around the implants occurs mainly in the neck and apical region [30,50, 57] affecting local bone physiology [24,26]. Some efforts were done in the past trying to alleviate this situation, such as the use of an intramobile-element [32,42,56], or a resilient collar around the implant neck [2], or even a cementum-periodontal ligament like formation around the implant [15,17,64].

Different geometries have been studied and attempts have also been made towards shape alteration, to improve the implant biomechanical performance [16,47,51–54,60]. The cuneiform geometry [21,22] is one of these. The purpose of this work was to compare, under the same conditions, the stress distribution around a cuneiform and a cylindrical threaded geometry implants, taking this later as a reference.

2. Material and methods

The methodology of the present study was based on previous work [22] which developed a model based on a complete edentulous human mandible.

2.1. Modeling

The geometric model of the mandible was obtained from a computerized tomography (Tomograph – Pro-Speed, GE, Medical Systems, Fairfield, CT, USA) of an actual human mandible according to Inou et al. [27] descriptions (Fig. 1a and 1b).

Table 1
Mesh Data

Geometry	Elements	Nodes	Degrees of Freedom
Cuneiform	17.193	26.708	80.134
Cylindrical threaded	15.386	23.899	71.696

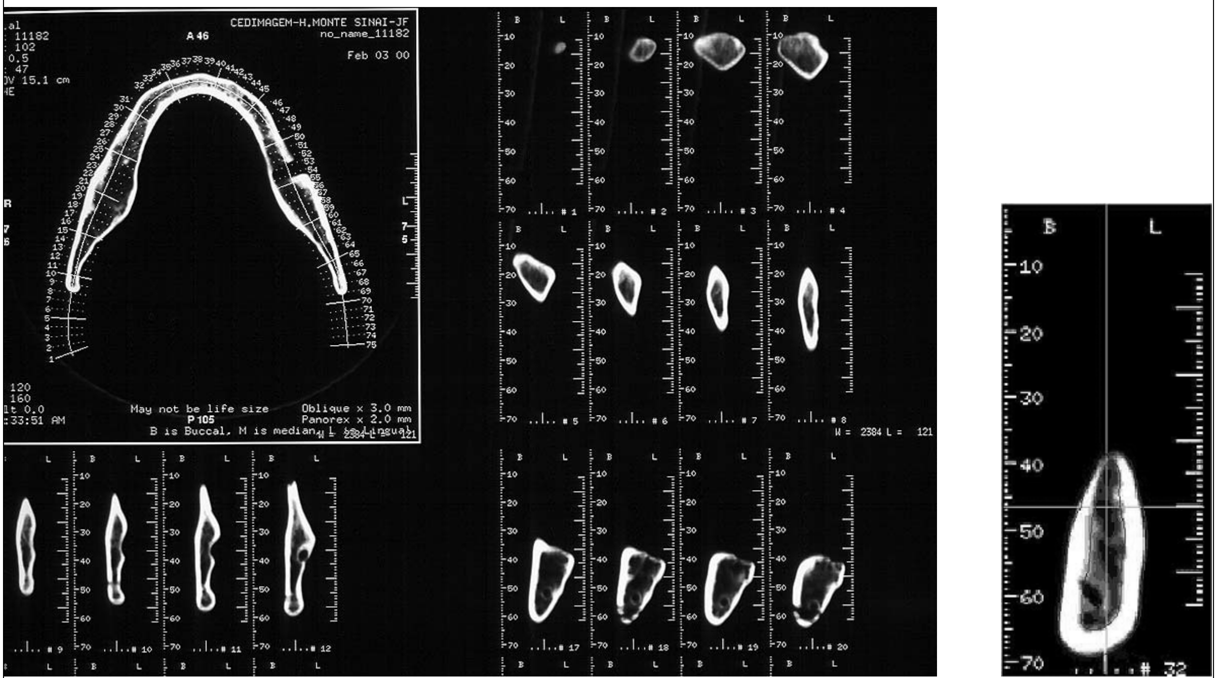

(a) (b)

Fig. 1. (a) Mandible CT scan. (b) Transverse section # 32, implant location.

The images were converted into digital data with the help of a scanner and transferred to the CAD program (AutoCAD, AutoDesk Inc., San Rafael, CA, USA). The coordinates of the contouring points were extracted from these plots and joined to form partial volumes, which together defined the final geometry. This process converted the obtained data into a 3-D solid model (Fig. 1c and 1d).

The geometric model thus obtained was meshed by the ANSYS finite element program (Ansys Corporate, Canonsburg, PA, USA), using tetrahedral isoparametric quadratic elements composed by 4 triangular faces, 4 vertices and 10 nodes. The grid reached 85.800 elements with 362.610 degrees of freedom. On the left premolar region, between the sections #30 #34 of the tomography, where the implants were placed, since greatest numerical accuracy was desired in this area, a finer mesh was used with 67.120 elements, corresponding to 276.960 degrees of freedom.

2.2. Implant systems, load positioning and interface conditions

The implants were also meshed by the same program with refined meshes (Table 1). The dimensions herein used for the implants were chosen as close as possible to most FEM studies reported in the literature. The cuneiform geometry had 13 mm length and 4mm of platform diameter (Fig. 2) (Bioform

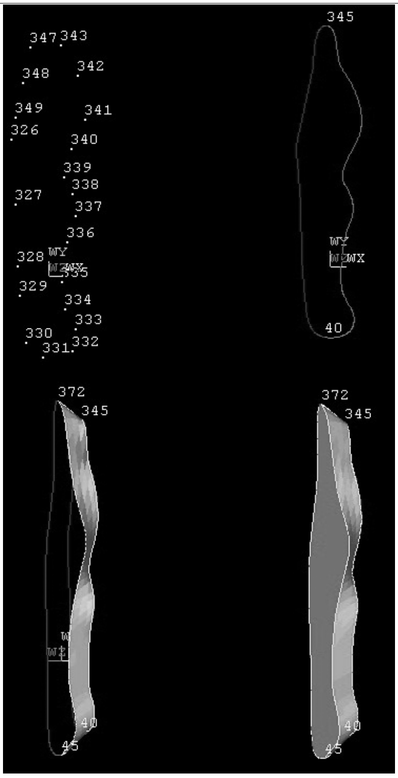

(c)

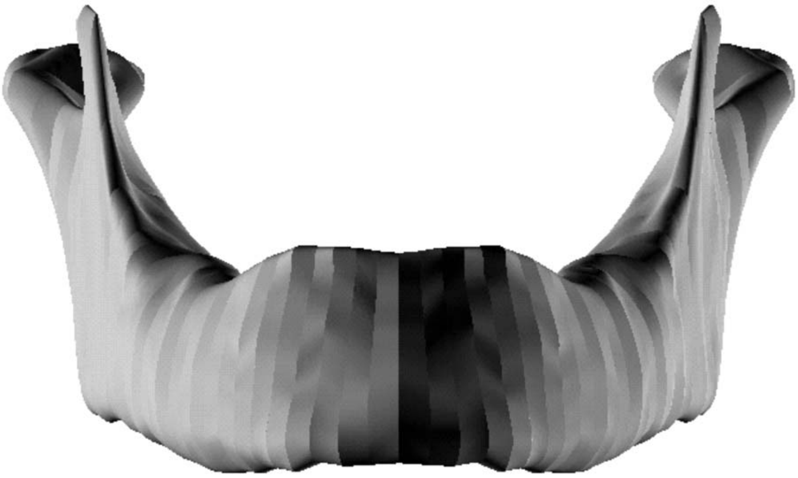

(d)

Fig. 1, continued. (c) Volumetric model of the geometry. (d) Computational geometric model of the mandible.

Implant, Maxtron Co., Juiz de Fora, MG, Brazil). The largest face of the implant body, presents three notches on each side to enhance mechanical retention during prosthetic management (Fig. 2).

The cylindrical threaded geometry modeled had (Nobel Biocare AB, Göteborg, Sweden) 13 mm

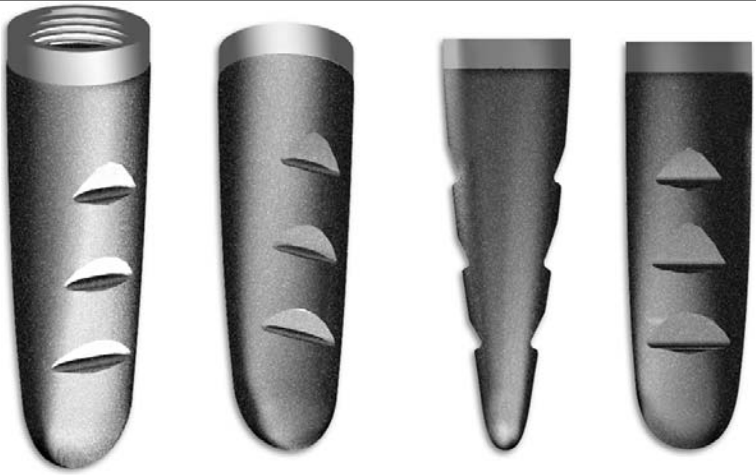

Fig. 2. Cuneiform implant.

length, 4 mm of platform diameter and 3.70 mm of body diameter. The small difference from the original manufactured dimensions: 0.1 mm on the platform and 0.05 mm on the body, attempted to bring the two geometries closer, for comparisons purposes.

A vertical load of 100 N was applied at the top of each implant in the direction of their long axes [18, 41,42,67]. A layer of compact bone contoured the implant neck and their body was embedded in the medullary bone (Fig. 3a, 3b). A fixed bond, that is, total osseointegration, between bone and implant along the whole interface was assumed, which meant that under the applied load on the implant, relative motion between bone and implant did not occur.

2.3. Load and supporting system

The complete model was supported by mastication muscles forces: Masseter (M), Medial Pterygoid (PM), Lateral Pterygoid (PL), Temporalis (T), together with the temporomandibular joints restraints. The forces generated by the mastication muscles were determined based on their transverse sections, as proposed by Inou et al. [27]. The data obtained from this reference indicates the following relationship between these muscle actions:

$$\mathrm{M} = 1.72\ \mathrm{PL} \quad \mathrm{T} = 0.99\ \mathrm{PL} \quad \mathrm{PM} = 1.15\ \mathrm{PL}$$

The complete model was restrained as shown in Fig. 4. Considering the axial load (P = 100 N) applied on top of the implants, the values for the muscular forces to keep the equilibrium of the system were obtained from the equation:

$$\left(r_{\vec{M}} \times 2\vec{M} + 2P\vec{M} \times r_{\vec{PM}} + 2P\vec{L} \times r_{\vec{PL}} + 2\vec{T} \times r_{\vec{T}} + \vec{P_0} \times r_{\vec{P_0}} \right) \cdot \vec{e} = 0$$

In this equation, r_M, r_{PM}, r_{PL}, r_T, r_P are the distance vectors from the load application points of the muscle forces M, PM, PL, T and of the axial implants loads, P_0, to the $\times$ (1–2) axis passing thru the top of the condyles. The symbol "$\times$" denotes the vector product, the symbol ($\bullet$) denotes the inner vector product and $\vec{e}$ is the unit vector in the condylar axis direction. The position of the muscular forces and axial load are given in vector form in Table 2.

Table 2
Distance vector components (mm)

Vector distance	X direction	Y direction	Z direction
r_M	0.0	28.07	33.01
r_T	0.0	30.61	5.27
r_{PL}	0.0	9.56	6.31
r_{PM}	0.0	27.67	38.97
r_{Po}	0.0	80.63	23.89

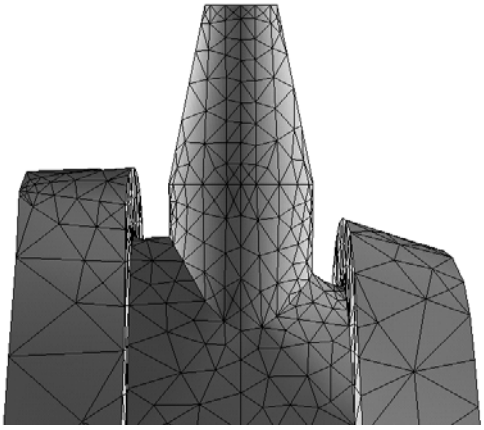

(a)

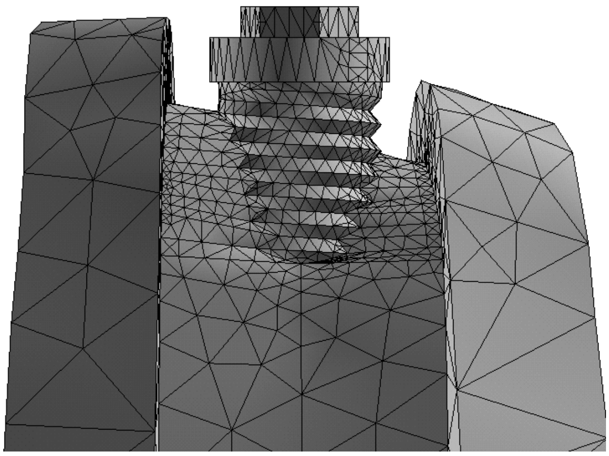

(b)

Fig. 3. (a) Cuneiform implant in the mandible without cortical layer. (b) Cylindrical threaded implant in the mandible (cortical layer and abutment not included).

According to descriptions found in the literature [48,35] the muscle positioning on the mandibular body was approximated and its resultant was considered acting on the centroid of the nodes of the elements faces, belonging to the muscular action area [49]. The forces directions are described in terms of director cosines, as given in Table 3. The values thus obtained from the equation and from the described force

Table 3
Director cosines of the resultant muscular forces (right side)

Muscle	Cos (α)	Cos (β)	Cos (γ)
Masseter	−0.043	−0.011	0.999
Medial pterygoid	0.587	−0.165	0.792
Lateral pterygoid	0.714	−0.692	0.106
Temporalis	−0.325	0.219	0.920

Table 4
Elastic properties of materials used

Material	Elasticity Modulus	Poisson's Ratio	References
Cortical bone	13.700 MPa	0.30	[4,9,16,19,20,38,40–42,46,61,62]
Medullary bone	1.370 MPa	0.30	[4,9,40–42,46,61,62]
Titanium	110.000 MPa	0.33	[6,38,61,62]

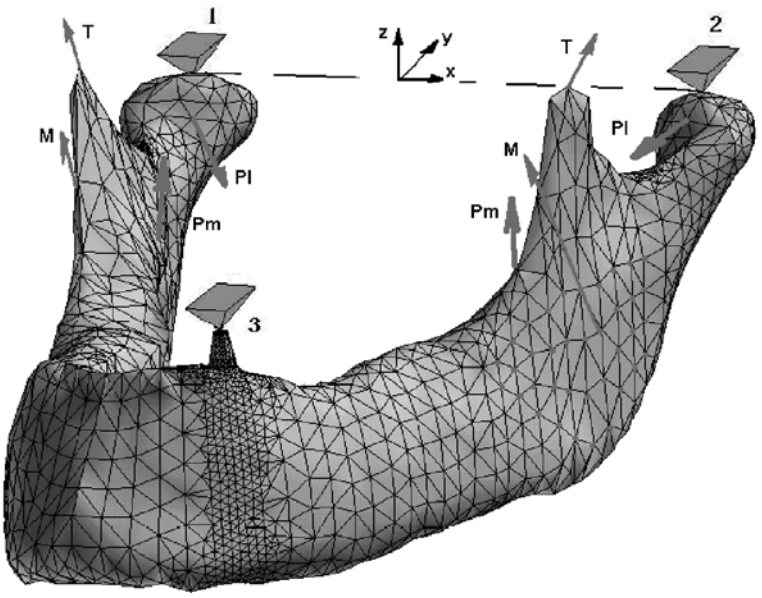

Fig. 4. Boundary conditions (red arrows indicate applied muscular forces).

relations between the muscular actions were:

$$M = 59.23\text{ N} \quad PM = 39.60\text{ N} \quad PL = 34.44\text{ N} \quad T = 34.09\text{ N}$$

The elastic properties of each material, such as cortical bone, medullary bone and titanium was extracted from current literature (Table 4).

The thickness of the cortical and medullary bone was assumed as defined by the X-ray CT sections of the mandible. The modeled bone was considered isotropic, homogeneous, and linearly elastic.

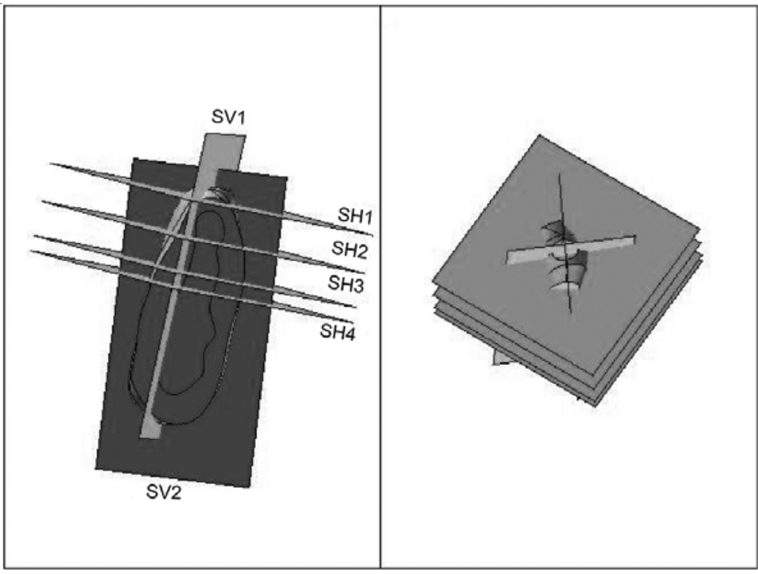

Fig. 5. Location of the horizontal and vertical sections.

3. Results

The analyses provided results for maximum (S1) and minimum (S3) principal stress and Von Mises (SEQV) stress field. Stress contours were color-coded and explained for each figure, where the stress values were indicated in Mega Pascal (MPa).

Global results showed mandibular deformation as described in literature and very similar stress distribution. For results visualization in the region close to the implants, sections of each implant were obtained in special points of interest. These sections were in four transverse (SH) and two longitudinal (SV) directions. The transverse sections were located as follow: SH4 was tangent to the apical area of the implant; SH3 was 2 mm from SH4 in the implant neck direction; SH2 was 4.5 mm from SH3 and SH1 was 5 mm from SH2, at the implant neck (Fig. 5). In implant neck region, at SV1 and SV2 sections, more detailed results were also shown.

Figures 6, 7, 8 show, respectively the S1, S3 and SEQV stress for those four transverse sections and for the longitudinal sections, including details of the implants neck region. Stress comparisons along implants contour lines (Fig. 9A and 9B) were drawn. The first one was transverse and contoured the implant neck region. Letters A, B, C, D were used to identify mesial, buccal, distal and lingual faces, respectively. The longitudinal lines profile of cuneiform implant were also positioned on these faces, mesial (A) buccal (B) distal (C) and lingual (D) and evaluated on the top, on the cortical-medullary bone joint (CT) on the first (#1) second (#2) and third (#3) re-entrance and on the apical region (#0). On the B-0 direction, six points were selected in order to show the stress in frontal implant surface. Due to its characteristics, the cylindrical threaded implant lines were positioned on top, on the first inferior edge of the platform (#1) on the angle between the platform and the body (#2) on the top of the first thread (#3) on the cortical-medullary bone joint (CT) and on the apical region (#0). The graphics plotted show the principal and Von Mises stress fields (Figs 10, 11, 12, 13 and 14).

The stress variation on the top (implant neck) displayed a similar pattern for both implants (Fig. 10). On both, stress concentration between the distal and lingual quarter occurred and the values were slightly higher for cylindrical threaded geometry. On the longitudinal sections, the stress also occurred with a

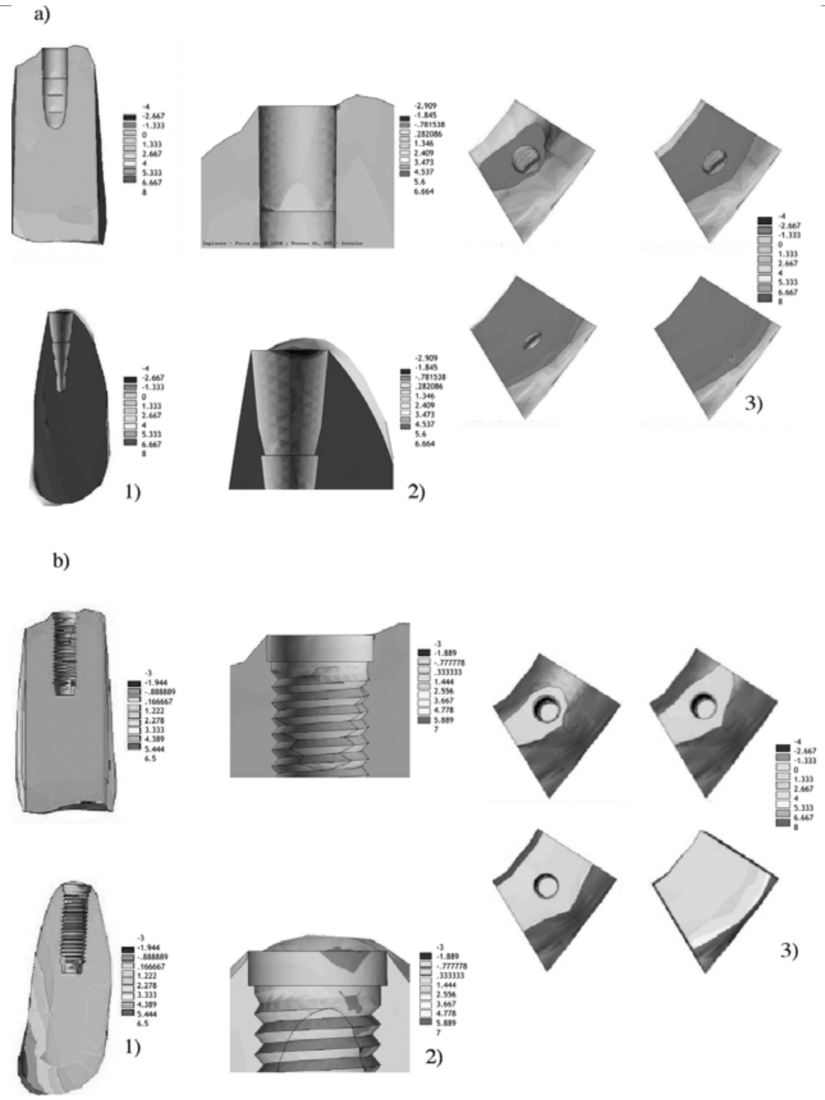

Fig. 6. Maximum principal stress – S1. 1) Axial sections 2) Detail of the top 3) Transverse sections. a) cuneiform, b) cylindrical threaded.

similar pattern (Figs 6–8). Difference was only observed at mesial area (A) with the stress concentration for cuneiform geometry at CT and for cylindrical threaded at #1. On distal top region (neck) (Figs 6–8), these concentration values were higher for cylindrical threaded implant. The graphics showed also the differences caused by the geometry along the body lines. For both implants no stress concentration areas occurred along the body length or at the apical area.

4. Discussion

Comparative analysis if under different modeling conditions could serve as a reference, but do not have conclusive value. However, the results of different studies can evidence a pattern of biomechanical

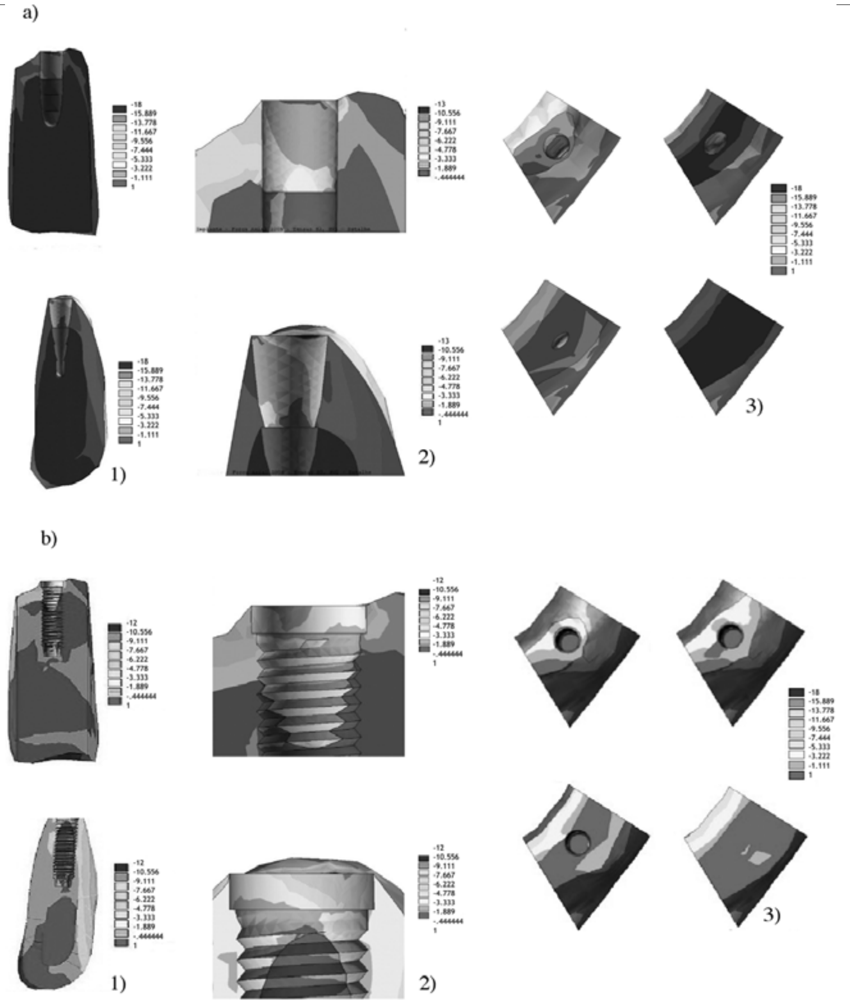

Fig. 7. Minimum principal stress – S3. 1) Axial sections 2) Detail of the top 3) Transverse sections. a) cuneiform, b) cylindrical threaded.

behavior and this occurred with cylindrical threaded geometry. This pattern be can used as a reference to study others implant geometries. This pattern established by cylindrical threaded implant has exhibited, under different analyses and conditions, stress concentration at the neck and at apical region [29,40–42, 51–53]. These stresses concentrations, however, in functional conditions, did not cause bone losses capable to lead to an implant fail, according to different authors [3,4,10–12,30,40]. The biomechanical behavior of this geometry, among other features, brings it to high levels of success [3,10–12].

Rieger et al. [53] and Inou et al. [27] related that in the regions where the stress concentration was out of physiologic limits, bone resorption occurred. Accordingly, in the regions where the stress was within physiologic levels, the bone kept its morphology. Both implant geometries stress here obtained were within the physiologic levels according to authors [19,20,24,52,54,55].

Studies comparing the cylindrical threaded geometry to other geometries concluded that the natural tooth and the conical geometry [23,51–54] had better biomechanical performance.

In a previous study, Cruz et al. [22] reported that cuneiform geometry presented reliable biomechanical

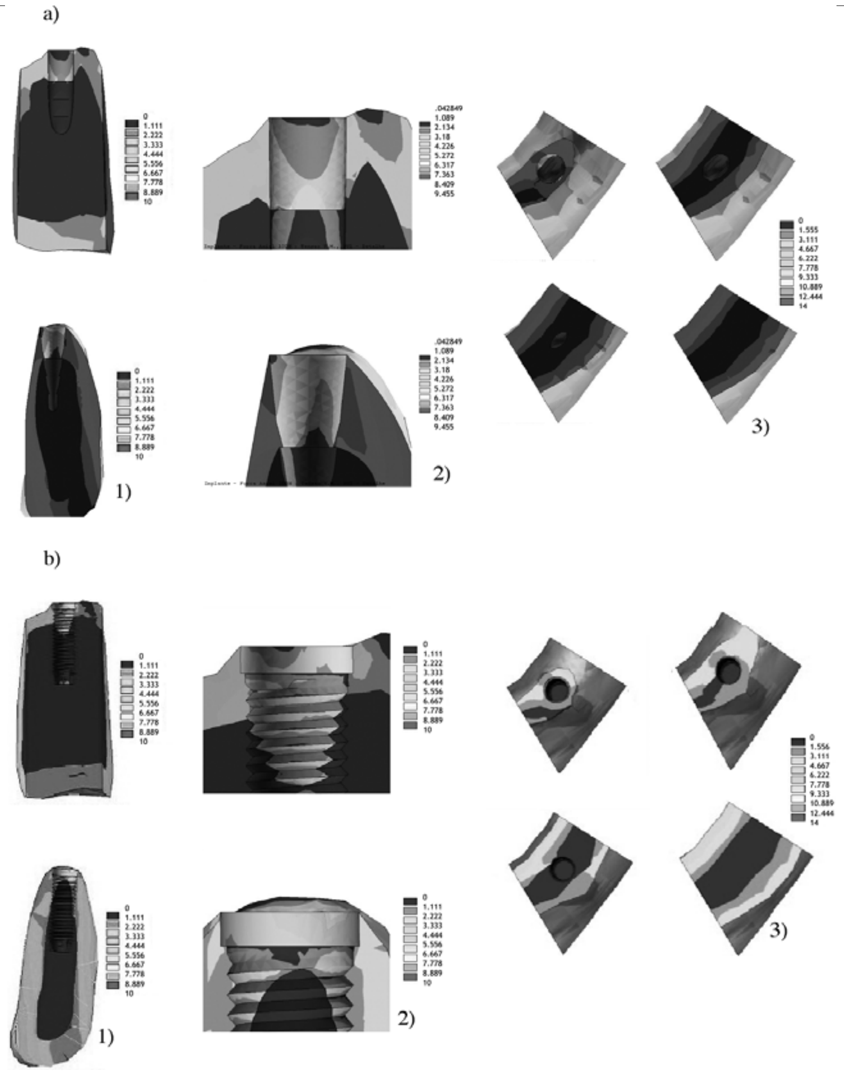

Fig. 8. Von Mises stress – SEQV. 1) Axial sections 2) Detail of the top 3) Transverse sections. a) cuneiform, b) cylindrical threaded.

behavior compared to other literature described results. The results of this work showed also that values of stress concentration were within the physiologic conditions described by others works [19,24,26,41, 42,51–54].

Both analyses here presented indicated the existence of a stress concentration at the same region of the neck, i.e., superior mesial area of the cortical layer. Bone losses in this area have been correlated to this stress concentration [4,9,18,41,51,53,57,64,66]. In this study, the stress concentration occurred only at one side and not all around the neck as previously related [4,18,30,52,54,57]. Rieger et al. [53] also described that the cylindrical geometry, induces relatively low stresses to the bone, along the body, concentrating stress near the neck and the apical region. This situation, according to them, can lead to pathologic bone losses at the middle implant region by atrophy and at the extremity by excessive stress. The cuneiform geometry implant here studied provided a smooth stress distribution inducing gradual

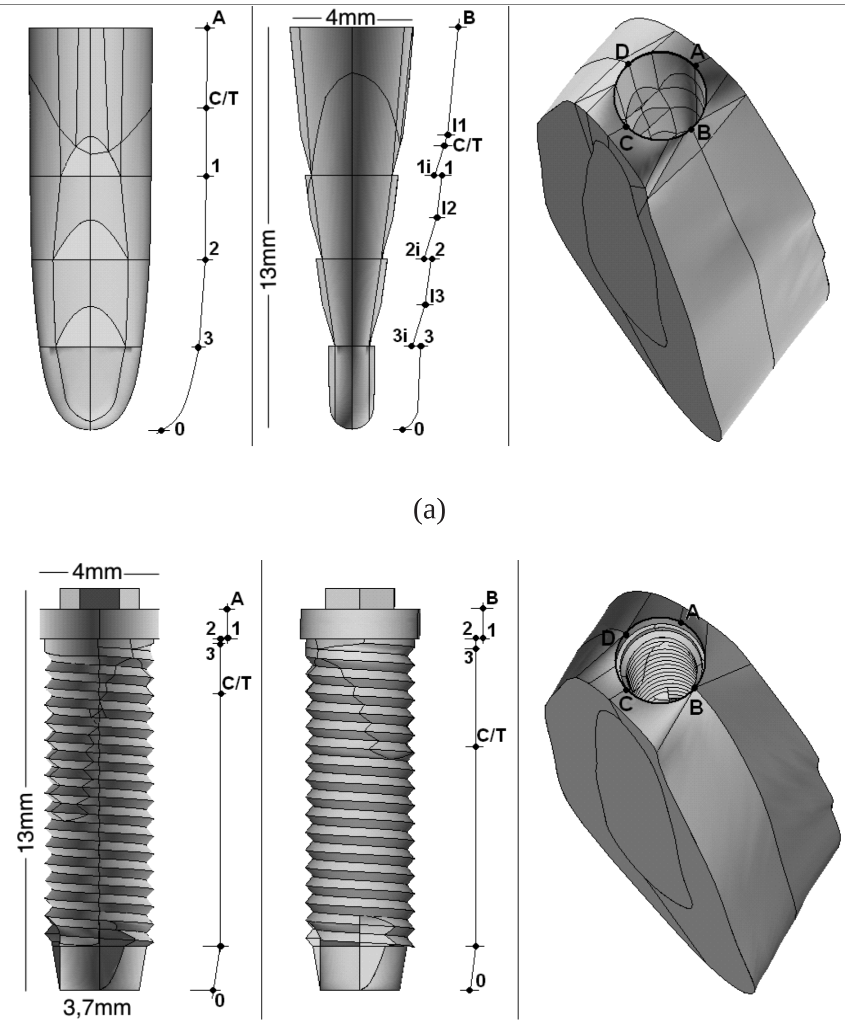

(a)

(b)

Fig. 9. (a) Cuneiform geometry diagram of lines. (b) Cylindrical threaded diagram of lines.

distribution of the load from the top to the apical region. No apical stress concentration occurred in the geometries here considered which is different from the results related in other studies that have frequently described an apical stress concentration [16,41,51,52,54,55].

5. Conclusions

Within the limitations of the present methodology, the obtained results indicated the following:

1. Both studied geometries presented quite similar qualitative stress distribution.
2. The stresses profiles along the implants length had specific pattern, reproducing the implant morphology.

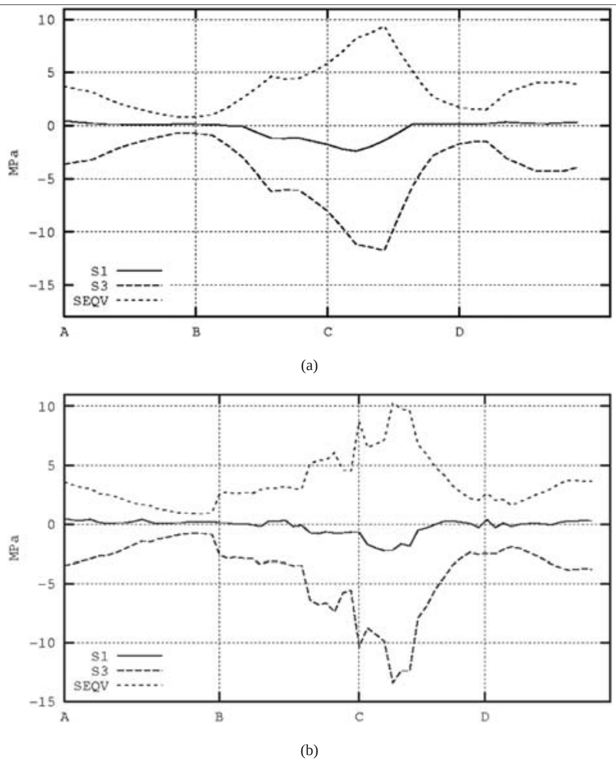

Fig. 10. Platform line. a) cuneiform, b) cylindrical threaded.

3. In both geometries occurred stress concentration at one side of the neck and no body or apical stress concentration.

Acknowledgments

This research was funded by grants from: SEBRAE (Federal Support Service for Micro Enterprises), State Department of Minas Gerais; Maxtron, Juiz de Fora, MG, Brazil; and it was supported by the School of Engineering, Federal University of Juiz de Fora (UFJF); the Research Center for Computational Methods in Engineering (NUMEC); the Regional Center for Innovation and Technology Transference (CRITT); the Clinical Center for Research in Stomatology (CLINEST); and the National Laboratory for Scientific Computing (LNCC). The first author is a scientific consultant for the Maxtron Company.

References

[1] Y. Çiftçi and S. Canay, The effect of veneering materials on stress distribution in implant-supported fixed prosthetic restorations, *Int J Oral Maxillofac Implants* **15**(4) (2000), 571–582.
[2] O.A. Abu-Hammad, A. Harrison and D. Williams, The effect of a hidroxyapatite-reinforced polyethylene stress distributor in a dental implant on compressive stress levels in surrounding bone, *Int J Oral Maxillofac Implants* **15**(4) (2000), 559–564.
[3] R. Adell, U. Lekholm, B. Rockler and P.-I. Brånemark, A 15-year study of osseointegrated implants in the treatment of the edentulous jaw, *Int J Oral Surg* **10** (1981), 387–416.

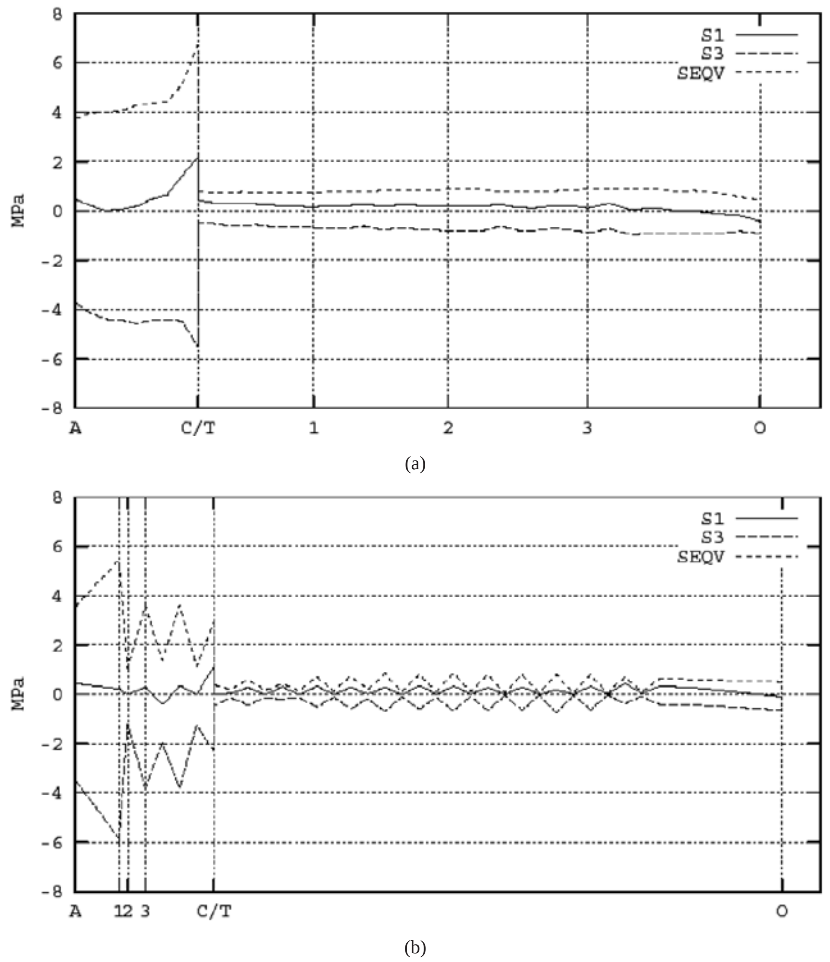

Fig. 11. Line 1. a) cuneiform, b) cylindrical threaded.

[4] I. Akpinar, F. Demirel, L. Parnas and S. Sahin, A comparison of stress and strain distribution characteristics of two different rigid implant designs for distal-extension fixed prostheses, *Quintessence Int* **27**(1) (1996), 11–17.
[5] T. Albrektsson and M. Jacobsson, Bone-metal interface in osseointegration, *J Prosthet Dent* **57**(5) (1987), 597–607.
[6] T. Baiamonte, M.F. Abbate, F. Pizzarello, J.L. Lozada and R. James, The experimental verification of the efficacy of finite element modeling to dental implant systems, *J Oral Implantol* **22**(2) (1996), 104–110.
[7] U.R. Benzing, H. Gall and H. Weber, Biomechanical aspects of two different implant-prosthetic concepts for edentulous maxillae, *Int J Oral Maxillofac Implants* **10**(2) (1995), 188–198.
[8] M.W. Bidez and C.E. Misch, Clinical biomechanics, in: *Contemporary Implant Dentistry,* C.E. Misch, ed., St Louis: Mosby, 1993, pp. 279–311.
[9] L. Borchers and P. Reichart, Three-dimensional stress distribution around a dental implant at different stages of interface development, *J Dent Res* **62**(2) (1983), 155–159.
[10] P.-I. Brånemark, R. Adell, U. Breine, B.O. Hansson, J. Lindstrom and A. Ohlsson, Intra-osseous anchorage of dental prostheses. I. Experimental studies, *Scand J Plast Reconstr Surg* **3**(2) (1969), 81–100.
[11] P.-I. Brånemark, B.O. Hansson, R. Adell, U. Breine, J. Lindström, O. Hallén and A. Öhman, Osseointegrated implants in the treatment of the edentulous jaw. Experience from a 10-year period, *Scand J Plast Reconstr Surg – Supple* **16** (1977), 1–132.
[12] P.-I. Brånemark, G.A. Zarb and T. Albrektsson, eds, *Tissue-Integrated Prostheses: Osseointegration in Clinical Dentistry,* Chicago: Quintessence, 1985, pp. 350.

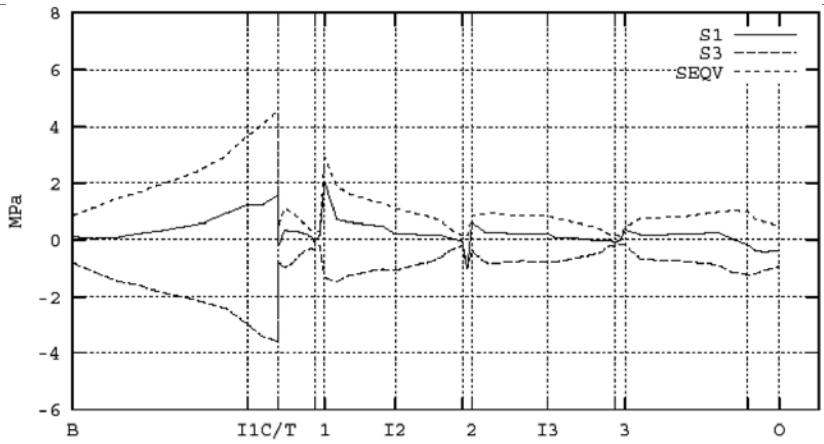

(a)

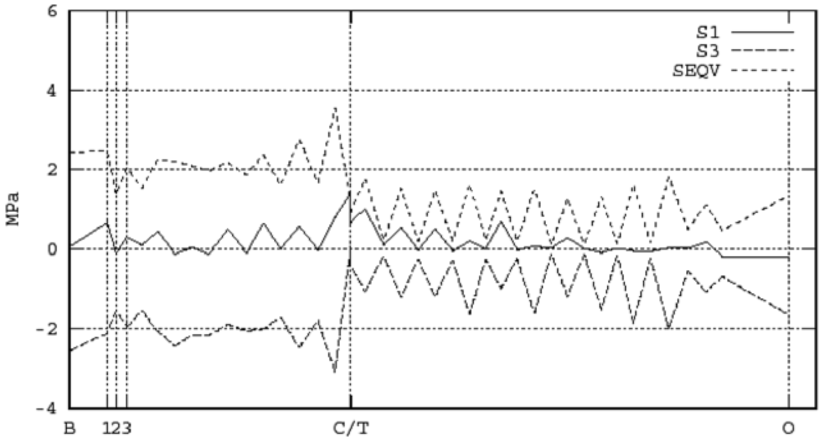

(b)

Fig. 12. Line 2. a) cuneiform, b) cylindrical threaded.

[13] J.B. Brunski, D.A. Puleo and A. Nanci, Biomaterials and biomechanics of oral and maxillofacial implants: Current status and future developments, *Int J Oral Maxillofac Implants* **15**(1) (2000), 15–46.
[14] J.B. Brunski, Biomaterials and biomechanics in dental implant design, *Int J Oral Maxillofac Implants* **3** (1988), 85–97.
[15] D. Buser, K. Warrer and T. Karring, Formation of a periodontal ligament around titanium implants, *J Periodontol* **61**(9) (1990), 597–601.
[16] S. Canay, N. Hersek, I. Akpinar and Z. Asik, Comparison of stress distribution around vertical and angled implants with finite-element analysis, *Quintessence Int* **27**(9) (1996), 591–598.
[17] B.H. Choi, Periodontal ligament formation around titanium implants using cultured periodontal ligament cells: a pilot study, *Int J Oral Maxillofac Implants* **15**(2) (2000), 193–196.
[18] N.L. Clelland, Y.H. Ismail, H.S. Zaki and D. Pipko, Three-dimensional finite element stress analysis in and around the Screw-Vent implant, *Int J Oral Maxillofac Implants* **6**(4) (1991), 391–398.
[19] S.D. Cook, J.J. Klawitter and A.M. Weinstein, A model for the implant-bone interface characteristics of porous dental implants, *J Dent Res* **61**(8) (1982), 1006–1009.
[20] S.D. Cook, A.M. Weinstein and J.J. Klawitter, A three-dimensional finite element analysis of a porous rooted Co-Cr-Mo alloy dental implant, *J Dent Res* **61**(1) (1982), 25–29.
[21] M. Cruz, C.C. Reis and F.F. Mattos, Implant-induced expansion of atrophic ridges for the placement of implants, *J Prosthet Dent* **85**(4) (2001), 377–381.

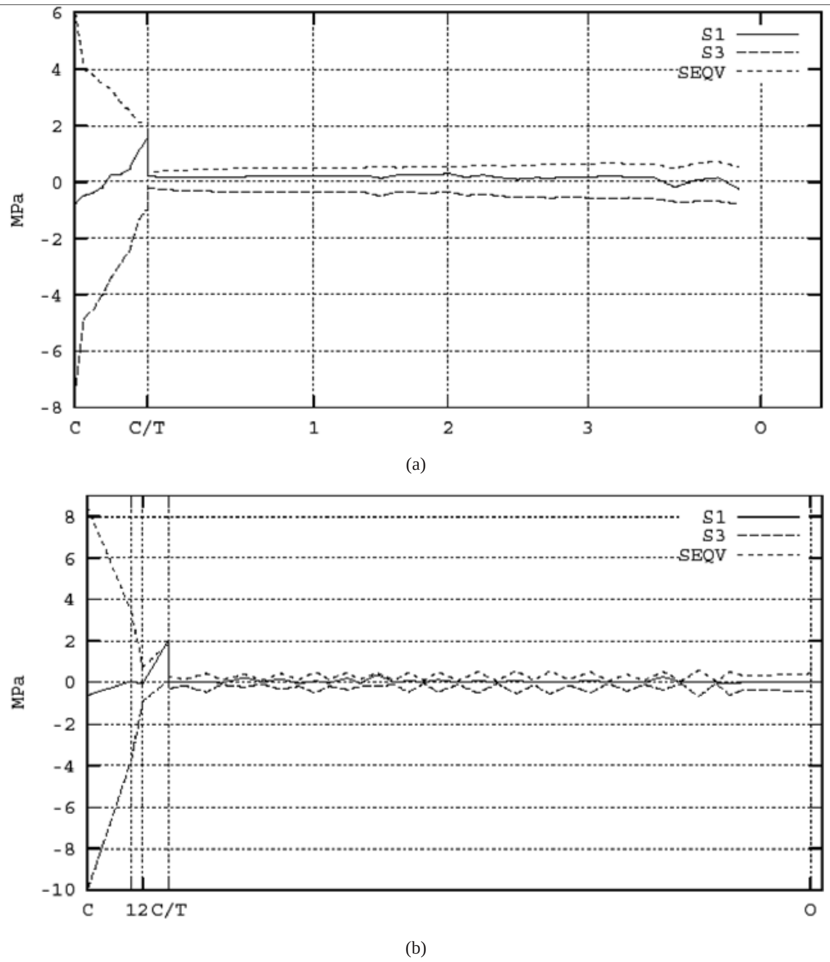

Fig. 13. Line 3. a) cuneiform, b) cylindrical threaded.

[22] M. Cruz, T. Wassal, E.M. Toledo, L.P.S. Barra and A.C.C. Lemonge, Three-dimensional finite element stress analysis of a cuneiform-geometry implant, *Int J Oral Maxillofac Implants* **18**(5) (2003), 675–684.

[23] D.N. Deines, J.D. Eick, C.M. Cobb, C.Q. Bowles and C.M. Johnson, Photoelastic stress analysis of natural teeth and three osseointegrated implant designs, *Int J Periodontics Restorative Dent* **13**(6) (1993), 541–549.

[24] C. Hassler, E.F. Rybicki, K.D. Cummings and L.C. Clark, Quantification of bone stresses during remodeling, *J Biomech* **13** (1980), 185–190.

[25] D.C. Holmes, W.R. Grigsby, V.K. Goel and J.C. Keller, Comparison of stress transmission in the IMZ implants system with polyoximethylene or titanium intramobile element: a finite element stress analysis, *Int J Oral Maxillofac Implants* **7** (1992), 450–458.

[26] S.J. Hoshaw, J.B. Brunski and G.V.B. Cochran, Mechanical loading of Brånemark implants affects interfacial bone modeling and remodeling, *Int J Oral Maxillofac Implants* **9**(3) (1994), 345–360.

[27] N. Inou, Y. Iioka, H. Fujiwara and K. Maki, Functional adaptation of mandibular bone, in: *Computational Biomechanics*, K. Hayashi and H. Ishikawa, eds, Tokyo: Springer-Verlag, 1996, pp. 23–42.

[28] H. Iplikçioglu, K. Akça, M.C. Çehreli and S. Sahin, Comparison of non-linear finite element stress analysis with in vitro strain gauge measurements on a morse taper implant, *Int J Oral Maxillofac Implants* **18**(2) (2003), 258–265.

[29] C.M. Jeong, A.A. Caputo, R.S. Wylie, S.C. Son and Y.C. Jeon, Bicortically Stabilized Implant Load Transfer, *Int J Oral Maxillofac Implants* **18**(1) (2003), 59–65.

[30] Y.-C. Jung, C.-H. Han and K.-W. Lee, A 1-year radiographic evaluation of marginal bone around dental implants, *Int J Oral Maxillofac Implants* **11**(6) (1996), 811–818.

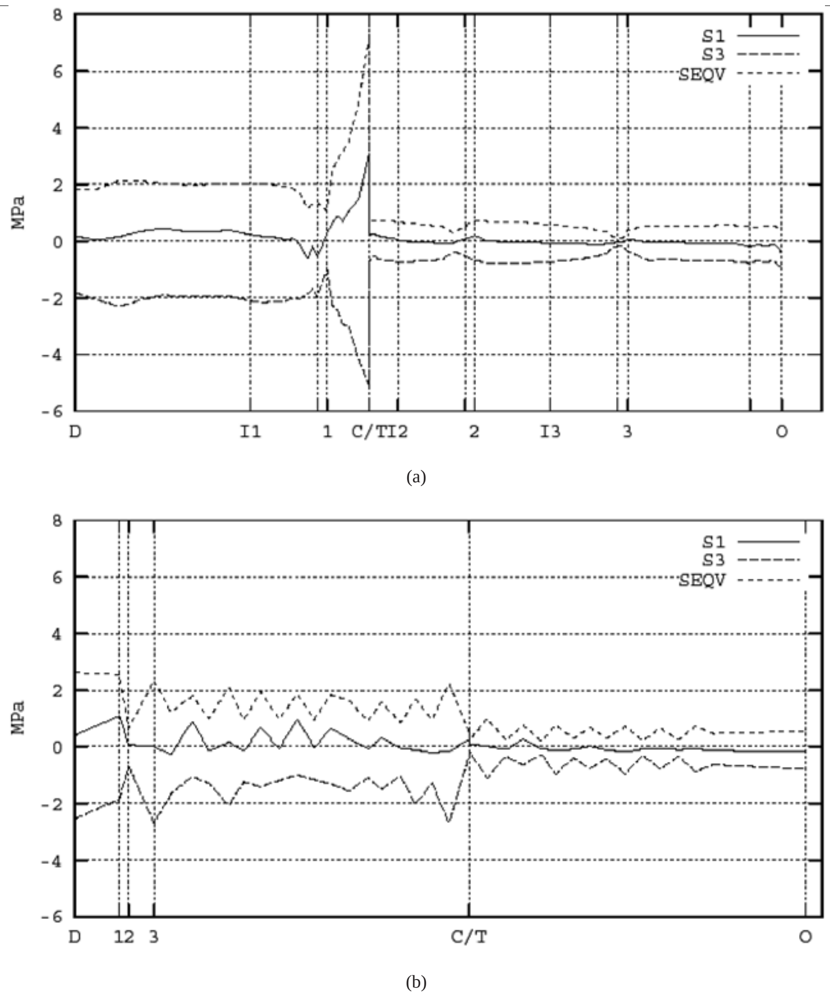

Fig. 14. Line 4. a) cuneiform, b) cylindrical threaded.

[31] J.H. Keyak, M.G. Fourkas, J.M. Meagher and H.B. Skinner, Validation of the automated method of three-dimensional finite element modeling of bone, *J Biomed Eng* **15** (1993), 505–509.
[32] A. Kirsch and P.J. Mentag, The IMZ endosseous two phase implant system: A complete oral rehabilitation treatment concept, *Oral Implantol* **XII**(4) (1986), 577–585.
[33] A.C. Knoell, A mathematical model of an *in vitro* human mandible, *J Biomech* **10** (1977), 159–166.
[34] J.H. Koolstra and T.M.G.J. Van Eijden, Application and validation of a three-dimensional mathematical model of the human masticatory system *in vivo*, *J Biomechanics* **25**(2) (1992), 175–187.
[35] J.H. Koolstra and T.M.G.J. Van Eijden, The jaw open-close movements predicted by biomechanical modeling, *J Biomech* **30**(9) (1997), 943–950.
[36] T.W.P. Korioth and A.G. Hannam, Deformation of the human mandible during simulated tooth clenching, *J Dent Res* **73**(1) (1994), 56–66.
[37] T.W.P. Korioth, D.P. Romilly and A.G. Hannam, Three-dimensional finite element stress analysis of the dentate human mandible, *Am J Phys Anthropol* **88** (1992), 69–96.
[38] I. Lewinstein, L. Banks-Sills and R. Eliasi, Finite element analysis of a new system (IL) for supporting an implant-retained cantilever prosthesis, *Int J Oral Maxillofac Implants* **10**(3) (1995), 355–366.
[39] C.-L. Lin and J.-C. Wang, Nonlinear finite element analysis of a splinted implant with various connectors and occlusal forces, *In J Oral Maxillofac Implants* **18**(3) (2003), 331–340.

[40] J.L. Lozada, M.F. Abbate, F.A. Pizzarello and R.A. James, Comparative three-dimensional analysis of two finite-element endosseous implants designs, *J Oral Implantol* **20**(4) (1994), 315–321.
[41] H.J.A. Meijer, J.H. Kuiper, F.J.M. Starmans and F. Bosman, Stress distribution around dental implants: Influence of superstructure, length of implants, and height of mandible, *J Prosthet Dent* **68**(1) (1992), 96–102.
[42] H.J.A. Meijer, F.J.M. Starmans, W.H.A. Steen and F. Bosman, Loading conditions of endosseous implants in an edentulous human mandible: A three-dimensional, finite-element study, *J Oral Rehabil* **23** (1996), 757–763.
[43] B.R. Merz, S. Hunenbart and U.C. Belser, Mechanics of the implant-abutment connection: An 8-degree taper compared to a butt joint connection, *Int J Oral Maxillofac Implants* **15**(4) (2000), 519–526.
[44] U. Meyer, H.-P. Wiesmann, T. Fillies and U. Joos, Early tissue reaction at the interface of immediately loaded dental implants, *In J Oral Maxillofac Implants* **18**(4) (2003), 489–499.
[45] W.M. Mihalko, T.C. May, J.F. Kay and W.R. Krause, Finite element analysis of interface geometry effects on the crestal bone surrounding a dental implant, *Implant Dent* **1** (1992), 212–217.
[46] W.M. Murphy, K.R. Williams and M.C. Gregory, Stress in bone adjacent to dental implants, *J Oral Rehabil* **22** (1995), 897–903.
[47] G. Papavasiliou, P. Kamposiora, S.C. Bayne and D.A. Felton, Three-dimensional finite element analysis of stress-distribution around single tooth implants as a function of bony support, prosthesis type, and loading during function, *J Prosthet Dent* **76**(6) (1996), 633–640.
[48] U. Posselt, *Physiology of Occlusion and Rehabilitation,* 2 ed., Oxford: Blackwell, 1964, 27–79.
[49] G.J. Pruim, H.J. Jongh and J. Ten Boschj, Forces acting on the mandible during bilateral static bite at different bite force levels, *J Biomech* **13** (1980), 755–763.
[50] T. Pylant, R.G. Triplett, M.C. Key and M.A. Brunsvold, A retrospective evaluation of endosseous titanium implants in the partially edentulous patient, *Int J Oral Maxillofac Implants* **7**(2) (1992), 195–202.
[51] M.R. Rieger, W.K. Adams, G.L. Kinzel and M.O. Brose, Finite element analysis of bone-adapted and bone-bonded endosseous implants, *J Prosthet Dent* **62**(4) (1989), 436–440.
[52] M.R. Rieger, W.K. Adams and G.L. Kinzel, A finite element survey of eleven endosseous implants, *J Prosthet Dent* **63**(4) (1990), 457–465.
[53] M.R. Rieger, K. Fareed, W.K. Adams and R. Tanquist, A Bone stress distribution for three endosseous implants, *J Prosthet Dent* **61** (1989), 223–228.
[54] M.R. Rieger, M. Mayberry and M.O. Brose, Finite element analysis of six endosseous implants, *J Prosthet Dent* **63**(4) (1990), 671–676.
[55] D. Siegele and U. Soltész, Numerical investigations of the influence of implant shape on stress distribution in the jaw bone, *Int J Oral Maxillofac Implants* **4** (1989), 333–340.
[56] H. Spiekermann, *Color Atlas of Dental Medicine: Implantology,* New York: Thieme, 1995, 36–45.
[57] R. Stegaroiu, T. Sato, H. Kusakari and O. Miyakawa, Influence of restoration type on stress distribution in bone around implants: A three-dimensional finite element analysis, *Int J Oral Maxillofac Implants* **13**(1) (1998), 82–90.
[58] N. Sykaras, A.M. Iacopino, V.A. Marker, R.G. Triplett and R.D. Woody, Implant materials, designs, and surface topographies: Their effect on osseointegration. A literature review, *Int J Oral Maxillofac Implants* **15**(5) (2000), 675–690.
[59] S. Tada, R. Stegaroiu, E. Kitamura, O. Miyakawa and H. Kusakari, Influence of implant design and bone quality on stress/strain distribution in bone around implants: A 3-dimensional finite element analysis, *Int J Oral Maxillofac Implants* **18**(3) (2003), 357–368.
[60] H. Vaillancourt, R.M. Pilliar and D. McCammond, Factors affecting crestal bone loss with dental implants partially covered with a porous coating: A finite element analysis, *Int J Oral Maxillofac Implants* **11**(3) (1996), 351–359.
[61] I.P. Van Rossen, L.H. Braak, C. Putter and K. Groot, Stress-absorbing elements in dental implants, *J Prosthet Dent* **64**(2) (1990), 198–205.
[62] P.P. Van Zyl, N.L. Grundling, C.H. Jooste and E. Terblanche, Three-dimensional finite element model of a human mandible incorporating six osseointegrated implants for stress analysis of mandibular cantilever prostheses, *Int J Oral Maxillofac Implants* **10**(1) (1995), 51–57.
[63] M. Wadamoto, Y. Akagawa, Y. Sato and T. Kubo, The three-dimensional bone interfaces of an osseointegrated implant. I: A morphometric evaluation in initial healing, *J Prosthet Dent* **76** (1996), 170–175.
[64] K. Warrer, T. Karring and K. Gotfredsen, Periodontal ligament formation around different types of dental titanium implants. I: The self-tapping screw type implant system, *J Periodontol* **64** (1993), 29–34.
[65] L.A. Weinberg, The biomechanics of force distribution in implant-supported prostheses, *Int J Oral Maxillofac Implants* **8**(1) (1993), 19–31.
[66] A.M. Weinstein, J.J. Klawitter, S.C. Anand and R. Schuessler, Stress analysis of porous rooted dental implants, *J Dent Res* **55**(5) (1976), 772–777.
[67] K.R. Williams and A.D.C. Williams, Impulse response of a dental implant in bone by numerical analysis, *Biomaterials* **18**(10) (1997), 715–719.